DX.DOI.ORG//10.19199/2023.170.1121-9041.035

# A VEM application to geomechanical simulations for underground fluid storage

Alice Raeli*
Cristina Serazio*
Francesca Marcon**
Andrea Borio**
Nacer Benlalam*
Stefano Berrone**,***
Francesca Verga*

* DIATI, Dipartimento di Ingegneria dell'Ambiente, del Territorio e delle Infrastrutture, Politecnico di Torino, Torino (TO) ITALY
** DISMA, Dipartimento di Scienze Matematiche "Giuseppe Luigi Lagrange", Politecnico di Torino, Torino (TO) ITALY
*** Memeber of INdAM-GNCS

Corresponding author:
alice.raeli@polito.it

*In this paper, we discuss how to describe the geomechanical behavior of geological formations used for underground fluid storage through the application of the Virtual Element Method (VEM) on conforming polyhedral meshes for the solution of stress-strain equilibrium equations. Under the assumption of small deformations, the solution algorithm for an Isotropic Linear Elastic (ILE) constitutive law coupled with the Mohr-Coulomb perfectly plastic yield criterion is implemented. The solution is then tested on a geological scenario with simplified geometry but realistic rock parameters. Results are compared with the solution of a first-order FEM obtained from a commercial solver, showing a good agreement in terms of displacement and stress maps. In the current implementation, a stabilization term of the VEM projectors is tailored to the elastoplastic law, paving the way for the generalization to polyhedral grids and the introduction of domain discontinuities such as faults.*

***Keywords***: *underground fluid storage, virtual elements method (VEM), geomechanical simulation, plastic subsoil deformations, underground energy systems.*

## 1. Introduction

Natural gas storage in geological formations can play a fundamental role in the transition to a decarbonized and more sustainable energy future (Benetatos *et al.*, 2021). In the last decades, wide experience has been gained in the underground storage of natural gas (Verga, 2018) and $CO_2$ capture, utilization and geological sequestration (Bellini *et al.*, 2022; Benetatos *et al.*, 2021; IEA, 2020; Liu *et al.*, 2023). More recently, large-scale storage of chemical energy has been approached with increasing interest. Indeed, hydrogen stands out as a promising energy carrier since it holds the potential for megaton-scale storage, equivalent to terawatt-hours (TWh) of energy, within deep geological formations such as depleted gas/oil reservoir, salt caverns and brine-saturated porous rocks (Hematpur *et al.*, 2023; Miocic *et al.*, 2023; Shi *et al.*, 2020; Vasile *et al.*, 2023). Given the extension and complexity of the underground geological systems in terms of geometry, stratigraphy, lithology, and rock characterization, as well as the multi-physic nature of storage problems typically involving fluid flow in porous media, geochemical interactions between rock and fluids, and rock deformation, coupled 3D numerical models are required to simulate the system response (Benetatos *et al.*, 2017, 2021; Ramesh Kumar *et al.*, 2023). Both current regulations and public concerns call for geomechanical analyses to assess the system safety in terms of stored fluids containment and potentially induced micro-seismic and subsidence phenomena (Benetatos *et al.*, 2023; Fibbi *et al.*, 2023; Paluszny *et al.*, 2020). Thus, one of the main issues to address is the coupled modeling of fluid dynamics and geomechanics. To this end, a key aspect is the selection of the most representative constitutive stress-strain relation, describing deformations (strain) induced by an external force (stress).

Elasticity is the property of solid material to deform under the application of an external force and to recover its original shape after the force is removed (Fjær *et al.*, 2008). In the case of geological storage, the external force is the pore pressure variation occurring when fluids are injected underground. In relatively shallow unconsolidated formations pore pressure variations can cause significant volume reduction/increase, which in turn can lead to reversible subsidence/rebound phenomena (Benetatos *et al.*, 2020; Codegone *et al.*, 2016; Coti *et al.*, 2018; Ferronato *et al.*, 2013; Teatini *et al.*, 2011). Conversely, according to the theory of plasticity solids subject to loading conditions may sustain permanent deformations when completely unloaded. (Krabbenhøft, 2002; Neto *et al.*, 2008; Szymanski, 1996).

The project we developed is dedicated to the application of Virtual Element Methods (Beirão da Veiga *et al.*, 2013a, 2015), a

If there are references to colour figures in the text, the articles are available in open-access mode on the site www.geam-journal.org

generalization of traditional conforming finite elements (FEM), to the solution of the equilibrium equation coupled with an elastoplastic constitutive law to determine the deformations induced by pore pressure variations in a deep geological formation. The core of the problem is to opportunely discretize the rock volume and calculate the displacement maps on the identified nodes. One of the peculiarities of VEM, which makes it preferable over a classical FEM approach, is that the test and trial functions are not explicitly defined inside the polygons in the VEM space. This makes the formulation simpler and easily generalized to polyhedral elements. However, a stabilization term in the shape functions, in the form of the projector, needs to be introduced to assure the stability of the method. Stabilization criteria are strongly problem-dependent and represent one of the intrinsic difficulties of the method. Here we present the two alternatives that we elaborated for the stress-strain equilibrium equations applied to ILE constitutive law coupled with Mohr-Coulomb yield criteria in the underground fluid storage context. The two stabilization terms are suited for elastic and plastic simulations such that the results are in the same order as the local cell operator (Ahmad *et al.*, 2013; Beirão da Veiga *et al.*, 2017). The general theoretical framework presented refers to previous works (Beirão da Veiga *et al.*, 2013b; Benedetto *et al.*, 2014; Benlalam *et al.*, 2022; Berrone *et al.*, 2021a, 2021b; Berrone and Raeli, 2022; Gain *et al.*, 2014; van Huyssteen *et al.*, 2022).

The implemented model has already been successfully applied to stress-strain simulations under the ILE hypothesis in previous works (Benlalam *et al.*, 2022; Serazio, 2021). The discretization approach is based on conforming general meshes. In this paper the elastoplastic problem, with a focus on the implemented constitutive law, is presented, followed by the first interpolation order VEM implementation. An injection test on a synthetic reservoir with a simplified geometry (disk-shaped) is then discussed. Results, in terms of stress and displacement variations induced by a pore pressure increment, are verified via a commercial FEM solver for geomechanical simulations largely used in the oil and gas industry.

## 2. The Problem Model

### 2.1. Stress and Strain

We briefly recall the theoretical fundamentals necessary for the presented application. Refer to (Fjær *et al.*, 2008; Lancellotta, 2008; Neto *et al.*, 2008) for further details.

Cauchy's Theorem and the following theory show that the complete stress state of a point in $R^3$, within a continuous medium, can be represented by a second-order tensor ($\sigma$) called *Cauchy stress tensor* or *simply stress tensor*. It is possible to prove that $\sigma$ is symmetric and if the characteristic equation of the stress tensor is solved for a generic point of the continuum medium three orthogonal planes are identified, called principal planes, on which only normal stresses act. The normal stresses acting on these planes are called principal stress and are indicated as: $\sigma_1$ (maximum principal stress), $\sigma_2$ (intermediate principal stress), and $\sigma_3$ (minimum principal stress).

Focusing on the analysis of small deformations, the state on each point of the continuum medium is represented through a second-order tensor called *infinitesimal strain tensor* ($\varepsilon$). Its definition arises from the *Cauchy-Green tensors* of deformation, and it has the following expression:

$$\varepsilon = \frac{1}{2}\left(\nabla u + \nabla u^T\right) \qquad (1)$$

where $u$ is the displacement vector. $\varepsilon$ is symmetric, thus only 6 components are independent ($\varepsilon_{ij} = \varepsilon_{ji}$).

The planes on which only longitudinal deformations act ($\varepsilon_{ij} = 0$) can be derived. Analogously to the stresses, they are called principal strains: $\varepsilon_1$, $\varepsilon_2$, $\varepsilon_3$. In an isotropic medium, the directions of the main stresses and deformations coincide.

The stress caused by a fluid injection is modeled by an interaction between solid and fluid phases. Terzaghi's principle of effective stress (Terzaghi, 1936), initially developed for soils, constitutes the universally adopted law of interaction between phases and porous rocks (Bouteca and Guéguen, 1999) and it is expressed by the relation:

$$\sigma' = \sigma - \alpha p I \qquad (2)$$

where $p$ is the neutral pressure (or pore pressure), and $\alpha$ is called Biot's coefficient. The theoretical formalization of the effective stress concept and its generalization to three-dimensional problems were performed by Biot in the soil consolidation framework (Biot, 1941), which constitutes the basis of poroelasticity theory and it can be expressed as:

$$\alpha = 1 - \frac{K'}{K_S} \qquad (3)$$

where $K'$ is the frame modulus, i.e. the bulk modulus of the solid skeleton, and $K_S$ is the bulk modulus of the rock grains. Since $K' << K_S$, $\alpha$ is assumed to be equal to unity (Geertsma, 1973).

In the following, we will refer to the stress as the effective one with $\alpha$ fixed to one, concerning the code implementation. The ini-

tial effective stress configuration is also given as an initial equilibrium condition.

### 2.2. Linear Momentum Balance Equations

In the introduced framework and under the hypothesis of infinitesimal deformations and quasistatic conditions, the linear momentum balance problem can be expressed as:

$$\begin{cases} \nabla\cdot\sigma'(u) = -\nabla\cdot(\Delta p I) & in\ \Omega \\ u = 0 & on\ \Gamma^D \\ \sigma'\cdot n = 0 & on\ \Gamma^N \end{cases} \quad (4)$$

where Ω represents the domain and Γ its boundary, with Dirichlet (D) and Neumann (N) partitions, respectively. The goal of the resolution of the equilibrium equations is to produce a displacement vector ($u$) such that the associated effective stresses ($\sigma'$) balance the pore pressure variations $\Delta p$.

To sum up the problem, it is necessary to introduce a constitutive equation that aims to model the relation between strain and stresses, the specific one used in this project is briefly described in the following.

### 2.3. The Elastoplastic Model

In the project, the implemented constitutive model, i.e. the relation between stress and strain, is a homogeneous isotropic linear elastic (ILE) model coupled with a perfectly plastic (i.e. no hardening law) yield surface, defined by Mohr-Coulomb failure criteria with the non-associated plastic flow (i.e. the yield surface and the plastic potential do not coincide) (Abbo *et al.*, 2011; Abbo and Sloan, 1995; Krabbenhøft, 2002; Neto *et al.*, 2008). The fundamental assumption of this elastoplastic theory is that the strain can be decomposed in the sum of an elastic or reversible component ($\varepsilon^e$) and a plastic or irreversible one ($\varepsilon^p$):

$$\varepsilon = \varepsilon^e + \varepsilon^p \quad (5)$$

Thus, the stress corresponding to a configuration with total strain ε is given by:

$$\sigma = D(\varepsilon - \varepsilon^p) \quad (6)$$

Where $D$ is the elastic constitutive matrix. In the elastic domain, the generalized Hooke's law describes the stress-strain relation in $R^3$:

$$\sigma' = 2\mu\varepsilon + [\lambda tr(\varepsilon) - \alpha p]I \quad (7)$$

where μ and λ are the Lamé Elastic Constants

$$\mu = \frac{E}{2(1+\nu)}$$
$$\lambda = \frac{E\nu}{(1+\nu)(1-2\nu)} \quad (8)$$

$E$ is Young's modulus and ν is Poisson's ratio. In general, the elastic domain is bounded by the yield stress function, above which plastic deformation takes place. Coulomb (Coulomb, 1776) postulated that the shear strength of rocks and soils is composed of two parts: a constant cohesion $c$ and a friction component dependent on the normal stress (characterized by the friction angle ϕ). Following (Abbo *et al.*, 2011; Abbo and Sloan, 1995), we present the Mohr's-Coulomb yield criterion in terms of principal stresses with the assumption $\sigma'_1 \geq \sigma'_2 \geq \sigma'_3$. The general expression of the yield surface is reported in equation 9.

$$\Phi_{i_1,i_2}(\sigma') = (1-\sin(\varphi))\,\sigma'_{i_1} + \\ -(1+\sin(\varphi))\,\sigma'_{i_2} - 2c\cos(\varphi) \quad (9)$$
$$i_1, i_2 = 1,2,3 \qquad i_1 \neq i_2$$

It follows that its multi-surface representation in the space of the principal stresses is a pyramid with a hexagonal base and the axis coinciding with the hydrostatic ones, as shown in Figure 9.

When applying the Mohr-Coulomb yield criterion to rock materials, a non-associated plastic flow is usually introduced and a flow potential Ψ is defined. Such a choice is due to the necessity to control the dilatancy effect, usually overestimated by associative plastic flow. In the Mohr-Coulomb yield model, the flow potential is similar to the yield surface, i.e. the friction angle ϕ is substituted by the *dilatancy angle* ψ (Neto *et al.*, 2008; Fjær *et al.*, 2008):

Moreover, to ensure that the rotation of the coordinate system does not influence the conditions at which the material yields, criteria are expressed in terms of stress *invariants*. In particular, the *mean normal stress* has the expression

$$\sigma'_m = \frac{1}{3}(\sigma'_x + \sigma'_y + \sigma'_z) \quad (10)$$

the deviatoric stress component, instead

$$\bar{\sigma}' = \sqrt{J_2} \quad (11)$$
$$J_2 = \frac{1}{2}(s_x^2 + s_y^2 + s_z^2) + \tau_{xy}^2 + \tau_{yz}^2 + \tau_{xz}^2,$$

where $s_i = \sigma'_i - \sigma'_m$ are the deviatoric stresses.

The *Lode angle* (Han and Chen, 1987) is developed here in terms of the deviatoric stress component

$$\theta = \frac{1}{3}\sin^{-1}\left(\frac{-3\sqrt{3}}{2}\frac{J_3}{\bar{\sigma}'^3}\right). \quad (12)$$
$$J_3 = s_x s_y s_z + 2\tau_{xy}\tau_{yz}\tau_{xz} + \\ -s_x\tau_{yz}^2 - s_y\tau_{xz}^2 - s_z\tau_{xy}^2$$

We omit calculus details presenting a form of the Mohr-Coulomb criterion proposed by (Nayak and Zienkiewicz, 1972), the *Yield surface* (Φ) is expressed in function of stress invariants:

$$\Phi = \sigma'_m sin\varphi + \\ + \sqrt{\bar{\sigma}'^2\kappa^2(\theta) + a^2 sin^2(\varphi)} + \quad (13) \\ - c\cos(\varphi)$$

where

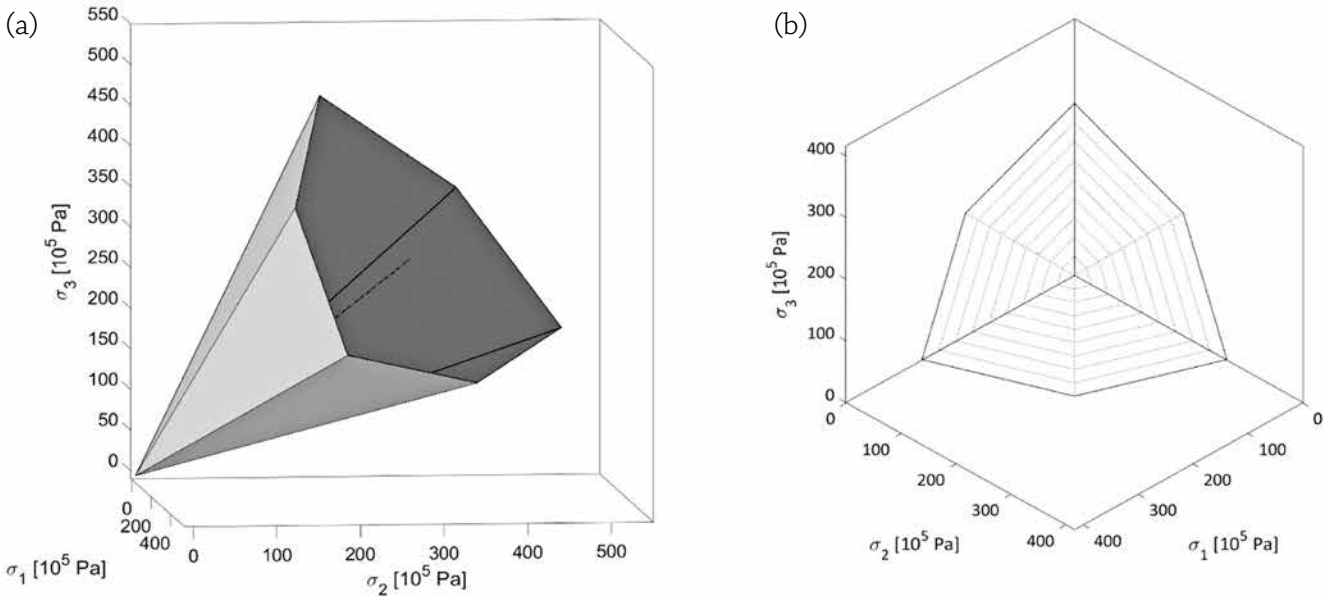


Fig. 1 – (a) Representation of the yield function defined by the Mohr-Coulomb criterion in the space of the principal stresses. As an example, c = 2.5 bar and ϕ = 25 ° where imposed. In (b) projection of the function on the deviatoric plane

$$\kappa(\theta) = \cos(\varphi) + -\frac{1}{\sqrt{3}}\sin(\varphi)\sin(\theta) \quad (14)$$

is a function controlling the shape of the surface in the plane orthogonal to the hydrostatic axis. The proposed formulation considers tensile stresses as positive. Furthermore, it is observed that in equation 13 a regularization term $a^2\sin^2(\phi)$ is introduced to make the Yield function C2 continuous in all stress states. In the following tests the parameter $a$ is set equal to 0.05 as suggested in (Abbo and Sloan, 1995). The interested reader is invited to refer to (Abbo *et al.*, 2011) for further details.

From the previous consideration, it follows that the general expression of the differential form of the constitutive law is

$$\dot{\sigma}' = D^{ep}\dot{\varepsilon} \quad (15)$$

where $D^{ep}$ represents the elasto-plastic constitutive matrix:

$$D^{ep} = D - \frac{D\frac{\partial \psi}{\partial \sigma'}\left(\frac{\partial \Phi}{\partial \sigma'}\right)^T D}{\left(\frac{\partial \Phi}{\partial \sigma'}\right)^T D\frac{\partial \psi}{\partial \sigma'}} \quad (16)$$

Equation 15 uniquely defines the stress increment due to a total strain increment. Moreover, $D^{ep}$ depends on the current stress state, thus introducing a non-linear relation in the discretized equilibrium equations.

## 3. VEM Discrete approximations

Under hypothesis of small deformation and generalized Hooke's law, the variational formulation of the model problem (4) has general expression

$$\text{find } u \in V: \quad a(u, v) = b(v), \forall v \in V \quad (17)$$

where $a(u, v) = \int_\Omega \sigma'(u)$: $\varepsilon(v) d\Omega$ is a bilinear form, $b(v) = -\int_\Omega \nabla \cdot (\Delta p I)\, v d\Omega$ the forcing term, $V := H^1_{0,\Gamma_D}(\Omega)$ the solution and test space and $(\cdot,\cdot)$ is the $L^2$-scalar product. Analogously to classical FEM, the solution of the model problem (17) through VEM is performed introducing a discrete approximation of the domain Ω, the space $V$, the bilinear form $a$ and forcing term $b$. Thus, a tessellation $\{T_h\}_h$ of Ω into disjoint non-overlapping convex polyhedral elements $P$ is introduced and, in accordance with the Galerkin approximation, it is possible to introduce a finite dimensional space $V_h \subset V$ with diameter $h$:

$$V_h = \{v_h \in V : v_{h|p} \in V_h(P), \forall P \in T_h\} \quad (18)$$

Then the symmetric bilinear form is split on each element $P(a^P)$

$$a(u_h, v_h) = \sum_{P \in T_h} a^P(u_h, v_h) \quad \forall u_h, v_h \in V_h \quad (19)$$

and the discrete model problem becomes

$$\text{find } u \in V_h: \quad a(u_h, v_h) = b(v_h), \forall v_h \in V_h \quad (20)$$

The solution of problem (20) requires the computation of the local stiffness matrix on each element, i.e., the calculation of weak form integrals through evaluation of interpolation functions. The core idea of VEM is to define an adequate (virtual) space $V_h$ such that it contains the polynomials of degree ≤ $k$ (where $k$ is the order of accuracy of the method), plus additional functions (in general not polynomials) that are never required to be computed thanks to the careful choice of degrees of free-

dom (DOFs) and the introduction of an approximation $a_h$ of the bilinear form. Operatively, it is necessary to construct a local projector on the space of polynomials of degree $\leq k$. In the following the order of accuracy $k$ is set equal to 1. Refer to (Ahmad *et al.*, 2013; Beirão da Veiga *et al.*, 2013a, 2016) for details on the construction of the local VEM space $V_h(P)$ and the derivation of $L^2(P)$-orthogonal projection operators. Here we recall its definition.

$$V_h^P = \left\{ \begin{matrix} v \in H^1(P) : \Delta v \in P_1(P), \\ v \in V_h^f, \forall f \in \partial P, \quad v \in C^0(\partial P) \end{matrix} \right\} \tag{21}$$

where $H^1(P)$ is the space of functions having a square-integrable gradient on $P$, $\partial P$ indicates the set of faces of the polyhedron, and $V_h^f$ is defined similarly to $V_h^P$, as follows:

$$V_h^f = \left\{ \begin{matrix} v \in H^1(f) : \Delta v \in P_1(f), \quad v \in P_1, \\ v \in P_1(e), \ \forall e \in \partial f, \ v \in C^0(\partial f) \end{matrix} \right\} \tag{22}$$

The approximation of the bilinear form has the form:

$$a_h^P(u_h, v_h) := a^{P,\nabla}(u_h, v_h) + S^{P,\nabla}(u_h, v_h)$$
$$\forall u_h, v_h \in V_h(P) \tag{23}$$

In the specific case the two terms have the expressions

$$a^{P,\nabla}(u_h, v_h) = \int_E \sigma'(\Pi^0_{0,P} \nabla u_h) : \varepsilon(\Pi^0_{0,P} \nabla v_h) dP \tag{24}$$

$$S^{P,\nabla}(u_h, v_h) = c_s S\left[(I - \Pi_{1,P})u_h, (I - \Pi^{\nabla}_{1,P})v_h\right]$$

where $\Pi^{\nabla}_{1,P}$ is the $H^1(P)$-orthogonal projection operator and $\Pi^0_{0,P}\nabla$ is $L^2(P)$-orthogonal projection operator of gradients onto constant, returning the integral mean of the gradient of a function. Projection operators on a generic $d$-dimensional object $E$ (i.e. $d = 2$ for polygon, $d = 3$ for polyhedron) are defined as

$$(\nabla p, \nabla \Pi^{\nabla}_{1,E} v)_E = (\nabla p, \nabla v)_E$$
$$\forall v \in H_1(E), \ \forall p \in P_1(E)$$
$$(1, \nabla \Pi^{\nabla}_{1E} v)_{\partial E} = (1, v)_{\partial E}, \forall v \in H^1(E)$$
$$\Pi^0_{0,E} \nabla : H^1(E) \to P_0(E)$$
$$\text{such that} \left( p, \Pi^0_{0,E} \frac{\partial v}{\partial x_i} \right)_E = \left( p, \frac{\partial v}{\partial x_i} \right)_E, \ \forall v \in H^1(E), \forall p \in P_0(E) \tag{25}$$

Where $P_0(E)$ is the space of constant-valued functions. From the definition of the projector's operators, it follows that for any function in the space $V_h^P$ it is possible to compute the above operators knowing only the values of the function at the vertices of $P$, which are chosen as degrees of freedom of the space. More details can be found in (Beirão da Veiga *et al.*, 2014).

If $\chi_i(v)$ is the DOF operator, i.e. the evaluation of the i$^{th}$ degree of freedom of $v$ and a local basis function $\varphi_i \in V_h(P)$ such that $\chi_i(\varphi_j) := \delta_{ij}$, it follows Lagrange-type interpolation identity

$$v_h = \sum_{i=1}^{n_{DOF}} \chi_i(v_h) \varphi_i, \forall v_h \in V_h(P) \tag{26}$$

and consequently $S^{P,\nabla}$ is evaluated defining as (Beirão da Veiga *et al.*, 2013b, 2014; Gain *et al.*, 2014)

$$S^{P,\nabla}(u_h, v_h) = c_s \sum_{k=1}^{n_{vE}} \chi_k\left((I - \Pi^{\nabla}_1)u_h\right) \chi_k\left((I - \Pi^{\nabla}_1)v_h\right) \tag{27}$$

The presence of non-linearities affects the choice of the coefficient $c_s$ associated with the stabilization term $S^{P,\nabla}$. For the validation test in the elastic domain $c_s$ is set as constant and it is equal to $2\mu + \lambda$ (see equation 8). In the more general elastoplastic case, instead, it is defined cell by cell as the infinity norm of the deviatoric part of the tangent matrix $D^{ep}$ appearing in the linearized stress-displacement constitutive relation, that is computed by a return-mapping algorithm (see Equation 16 and Section 3.1). This new definition aims to guarantee the non-singularity of the matrix operator and, at the same time, to scale the contribution of the stabilization term accordingly with the plastic contribution.

In the following, some details on the implemented algorithms for the resolution of the equilibrium equation coupled with the non-linear constitutive problem are presented. The applied return-mapping algorithm (Neto *et al.*, 2008) for the constitutive initial value problem is quickly sketched in Section 4.

We also provide the implementation of a *state update procedure* similar to the one proposed by (Neto *et al.*, 2008) using a pseudo-time increment $[t_n, t_{n+1}]$ for the numerical integration of the rate elastoplastic evolution equation; the update procedure gives the stress $\sigma'_{n+1}$ at the end of the loading step as a function of the internal variables $\alpha_n$ of the previous increment and the current strains:

$$\sigma'_{n+1} = \hat{\sigma}(\alpha_n, \varepsilon_{n+1}) \tag{28}$$

Where the functional $\sigma\hat{}$ assembles the internal force vector. In the current implementation, the internal variable $\alpha_n$ encodes information on the previous state of equilibrium. Indeed, when plastic deformation occurs at each loading step the updated material stress state depends on the previous ones, forming the so-called stress path. It follows that to set up a geomechanical simulation it is necessary to provide the *in situ* stress state, i.e. initial equilibrium stress map associated with the investigated volumes. Formally such a state needs to consider the depositional/erosional history of the sedimentary basin. Different models have been proposed to characterize such maps and several studies were dedicated to the assessment of the main parameter values. Within the litho-

$\Delta u^0 = 0, u = 0$
**for** n = 1 to *NLoads* **do**
  assembling $K^n$ and $f^n$
  $u_0 = 0, \epsilon_r = || f^n ||_2$
  **while** i < $I_{max}$ and $\epsilon < Tol$ **do**
    compute $u_i$ from $K^n u_i = f^n$
    solution control → *Line Search Algorithm*
    $\Delta u^n = \Delta u^n + u_i$
    assembling $K_i$ and $f_i$
    compute $\epsilon = \frac{||f_i||_2}{\epsilon_r}$
  **end**
  update stress state $\sigma'_n = \sigma'_{n-1} + \Delta\sigma'_n$
  $u_n = u_{n-1} + \Delta u^n$
**end**

Fig. 2 – Newton's Iterative Scheme for the resolution of the equilibrium equation.

$\delta u = \Delta u^n$
$\delta u_0 = \Delta u^n$
assign the starting solution obtained by *Newton Solve* $u_s = u_i$
set the residual $r = f_i, \alpha = 1, \beta = 10^{-4}$
**while** $j < maxIts$ *and* $\epsilon > Tol$ **do**
  $\delta u_j = \delta u + \alpha u_s$
  assemble $K_j, f_j$
  compute $\epsilon = \frac{||f_j||_2}{\epsilon_r}$
  check the Armijo condition
  $\frac{1}{2} f(\delta u_j)^T f(\delta u_j) \leq \frac{1}{2} f(\delta u)^T f(\delta u) + \beta\alpha\nabla f(\delta u)^T$
  If *true* then
    $j = maxIts$
  **else**
    $\alpha = 0.5\,\alpha$
    $j++$
  **end**
**end**

Fig. 3 – Line Search Algorithm associated with Newton Iteration.

sphere, stress is conventionally described by three main components of compressive stress: a vertical component ($\sigma_v$) and two horizontal components, corresponding to the maximum horizontal stress ($\sigma_H$) and the minimum ($\sigma_h$). In the following, assuming that the surface topography is regular and in absence of discontinuities, the three main components characterizing the *in situ* stress are supposed to coincide with the main stress axes. Moreover, the vertical component, called *lithostatic pressure*, depends on the weight of the overburden rock, i.e. thickness and nature of the sediments and saturating fluids as well as on the depositional history. Horizontal components instead are derived by exploiting correlations between components that have been proposed as a function of rock type and tectonic regime (Zang *et al.*, 2012).

In our specific case, the Newton Iterative algorithm proposed in (Krabbenhøft, 2002) for the resolution of equilibrium equations is implemented using a VEM (Beirão da Veiga *et al.*, 2013a, 2013b) formulation and that can be resumed in the algorithm sketched in figure 2.

*NLoads* is the number of loading steps set to split the imposed $\Delta p$ and the stress state $\sigma'$ is updated at the end of the process. The internal iterative algorithm stops when at least one of the two imposed conditions is true i.e. a maximum number of iterations is reached, or a tolerance value inequality is satisfied. In the presented tests the tolerance *Tol* is set equal to $10^{-3}$ and the maximum iterations parameter ($I_{max}$) is fixed to 25.

Furthermore, it is observed that Newton's method applied to the nonlinear elastoplastic problem does not ensure a reasonable convergence of the solution, thus, in the current version of the code, a *Line Search* backtracking algorithm is nested to Newton's cycle: an Armijo (Velez *et al.*, 2018) rule is applied to each step solution $u_i$ following the algorithm sketched in figure 3:

In our implementation β is a multiplier parameter and α is the control parameter applied to the current step solution. The maximum of iterations number *maxIts* is set equal to 10.

The forcing term is defined as the recorded difference in pore pressure due to injection/production operations.

### 3.1. Single-cell stress state update

As already introduced, the resolution of the elastoplastic constitutive problem requires the implementation of an iterative dedicated algorithm that aims to update the current stress state $\sigma'_A$ of each cell, singularly. In this specific case, a return mapping algorithm is coded following (Krabbenhøft, 2002).

Here the trial state of stress ($\sigma'_0$) is returned to the yield surface $\Phi(\sigma')$ on a point P, named *projected*, as sketched in figure 4.

In figure 5, the main steps of the coded algorithm are shown.

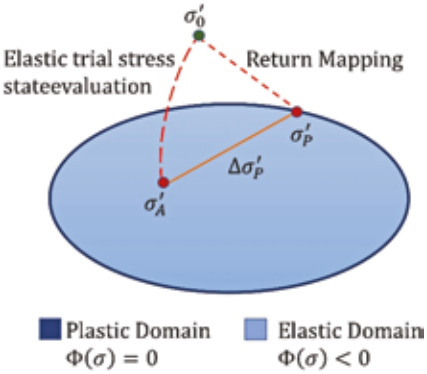


Fig. 4 – A sketch of the return mapping step.

$\sigma'_0 = \sigma'_A + \Delta\sigma'_e = \sigma'_A + D\Delta\varepsilon$
**while** $\Phi(\sigma'_{j+1}) < \epsilon$ **do**
  $\Delta\lambda = \frac{\Phi(\sigma'_j)}{\left(\frac{\partial\Phi}{\partial\sigma'_j}\right)^T D\left(\frac{\partial\Psi}{\partial\sigma'}\right)^j}$
  $\Delta\sigma'_P = \Delta\lambda D\left(\frac{\partial\Psi}{\partial\sigma'}\right)^j$
  $\sigma'_{j+1} = \sigma'_j - \Delta\sigma'_P$
**end**
**return** $\sigma'_P = \sigma'_A + \Delta\sigma'_P =$
$= \sigma'_A + \Delta\sigma'_e - \Delta\lambda D(\frac{\partial\Psi}{\partial\sigma'})^P$

Fig. 5 – Return Mapping Algorithm for the resolution for the initial value elastoplastic constitutive model.

In particular, Ψ is the gradient flow potential associated with the Mohr-Coulomb Yield surface. In this context, λ represents the Lagrangian Multipliers of the constrained problem.

### 3.2. Implementation Details

The code presented in this work is developed in collaboration with the Department of Mathematical Sciences of Politecnico di Torino. In particular, the library used to approximate the VEM formulation is developed by the GEOSCORE++ (https://areeweb.polito.it/geoscore/) team. The library is still an on-course project available on demand for interested developers.

The language used for the code implementation is C++ and *Eigen* (Guennebaud *et al.*, 2010) is the external library used to optimize matrix-vector products. The grid parser and the VEM solver import links to a later released version of VTK 9.2.0, meanwhile, the remaining external libraries (i.e. *Triangle* (Shewchuk, 1996) and *Eigen*) can be downloaded with the source.

A parameter *isPlastic* is used in the implementation to distinguish the constitutive law (plastic or not) associated with the current model. Such a parameter allows us to optimize the memory storage handling of large systems. When the problem is purely elastic the VEM operator matrix is symmetric thus only a triangular part of it is stored and computed by a *Preconjugate Gradient* solver. When plasticity can occur, the numerical operator is no more symmetric and the *Bi-conjugate Gradient* is applied. This implementation allows us to handle the elasticity efficiently in terms of CPU memory.

Tab. 1 – Disk-shaped reservoir model. Load term and elastoplastic constitutive model parameters.

| Parameter | Description | Value |
|---|---|---|
| $\Delta p$ | Imposed reservoir pore pressure variation | 2.5 $10^6$ Pa |
| $E$ | Young's Modulus | 2 $10^9$ Pa |
| $v$ | Poisson's Ratio | 0.25 |
| $\varphi$ | Friction angle | 25° |
| $c$ | Cohesion | 1.6 $10^5$ Pa |
| $\psi$ | Dilatancy angle | 5° |

### 3.3. Numerical Results

The validation of the implemented algorithm for the resolution of the elastoplastic constitutive model coupled with VEM is performed on an injection test on a synthetic reservoir with a simplified geometry as sketched in figure 6. This is a disk-shaped, isotropic and homogeneous reservoir (in red) with the vertical axis as the symmetry and thickness vs radius ratio (H/R) equal to 0.1. The relevant model parameters are listed in Figure 6. The Mohr-Coulomb yield surface is completely defined by two parameters, i.e. friction angle ($\phi$) and cohesion ($c$). Plastic flow is non-associated, thus a dilatancy angle ($\psi$) is assigned. No hardening parameters are set due to the perfect plasticity hypothesis. To force some nodes of the disk to reach plasticity it is necessary to impose a pore pressure variation of 25 MPa at a depth of 400 m (where the initial value is of the order of 4 MPa). The boundary conditions provide a null contribution from the lateral boundaries and the bottom face of the domain. The imposed pore pressure variation $\Delta p$ is given as an input parameter.

The investigated volume has an extension of 14 km × 14 km × 4.5 km and it is discretized in a structured hexahedral grid with a local refinement in the rectangular region reaching 4.3 $10^5$ nodes involving 1219779 degrees of freedom, corresponding to the number of rows of the numerical operator. The local grid refinement region is identified as the grey box in Figure 6. A FEM solution obtained from a commercial software is taken as a reference.

The simulation is set up assuming an initial stress equilibrium. As already discussed, in this specific case it can also be assumed that the three main components of the compressive stress $\sigma_V$, $\sigma_H$, and $\sigma_h$ coincide with the main stress axes. The vertical component depends

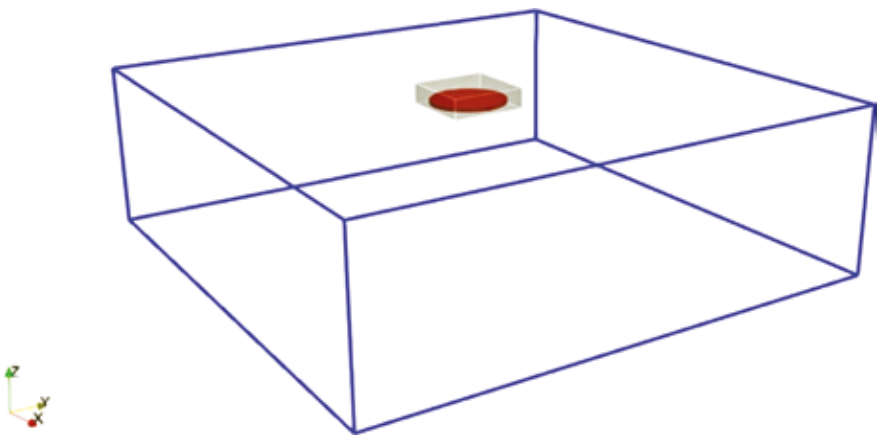

Fig. 6 – A sketch of the disk-shaped model.

on gravity, and it is related to the weight of the overburdened rock. The value of the $\sigma_H$ component is the most difficult to calculate and is typically derived from a direct correlation with the value of $\sigma_h$. Different correlations between, $\sigma_H$, $\sigma_h$ and $\sigma_V$ have been proposed as a function of the rock type and tectonic regime (Zang *et al.*, 2012). Referring to (Caporali *et al.*, 2018) it is possible to identify an area within the Po-plain basin where the trust faulting regime is dominant, i.e. $\sigma_H > \sigma_h > \sigma_V$. Under this assumption, the model is initialized as

$$\sigma_V = \sigma_{lithostatic}$$
$$\sigma_H = \sigma_h = 1.1\ \sigma_V \quad (29)$$

The forcing term $\Delta p$ is imposed on the reservoir cells. The load is divided into 5 steps of 5 $10^5$ Pa each. Accordingly, 3 steps occur in the linear-elastic domain and 2 steps occur in the plastic regime. Since the resolution of the model in the plastic regime introduces strong nonlinearities which make the convergence of the implemented iterative algorithm less efficient, the last step is further divided into 5 sub-increments of 1 $10^5$ Pa each, as sketched in figure 7.

The comparison between the solution computed by the FEM and VEM solver is performed in terms of domain cells that fail in the plastic domain. It is observed that the two regions essentially overlap, as shown in figure 8.

The comparison of the evolution of the stress path and yield function is performed on a selected probe cell (highlighted in yellow in figure 8) of the reservoir.

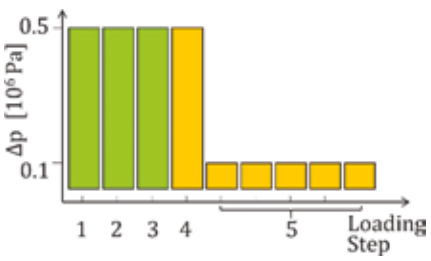


Fig. 7 – Loading step sequence.

A satisfactory match between the solutions calculated with the two methods is shown in figure 9: (a) the evolution of the yield function with respect to the loading steps is observed; (b) the stress path represented in terms of mean stress and deviatoric stress is depicted. In agreement with the FEM solution, the compression stress is here considered positive.

The comparison between the two solutions in terms of displacement field is performed at the surface (z = 0 m) along section HH', as shown in figure 10a where the colormap refers to the subsidence of the VEM solution expressed in m. In figure 10b the comparison of the z-direction displacement,

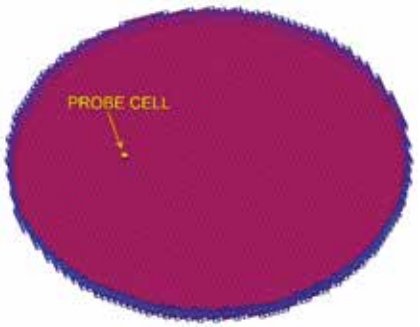


Fig. 8 – Comparison of cells in the plastic domain at the last loading step. FEM blue wireframe and VEM red surface.

calculated with the two methods along the HH' section, shows a satisfactory correspondence between the solutions.

Analogous colormap and plot are depicted for the displacement

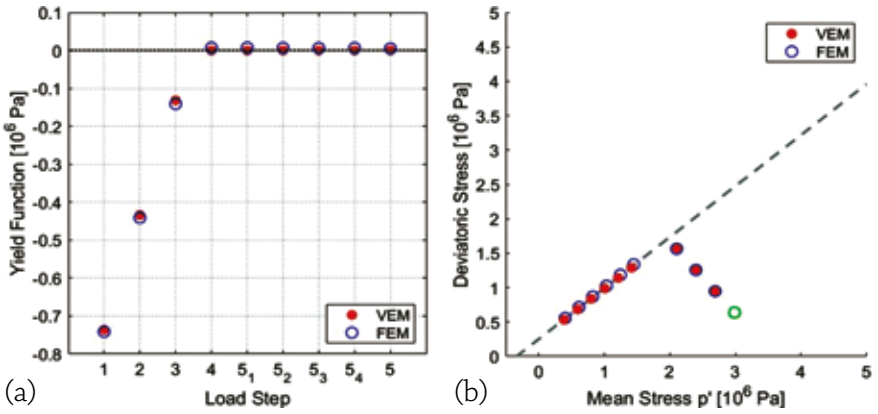


Fig. 9 – (a) Yield function evolution on probe cell with respect to loading step. (b) Stress path of the probe cell. Initial stress state in green and dotted line for the yield function projection.

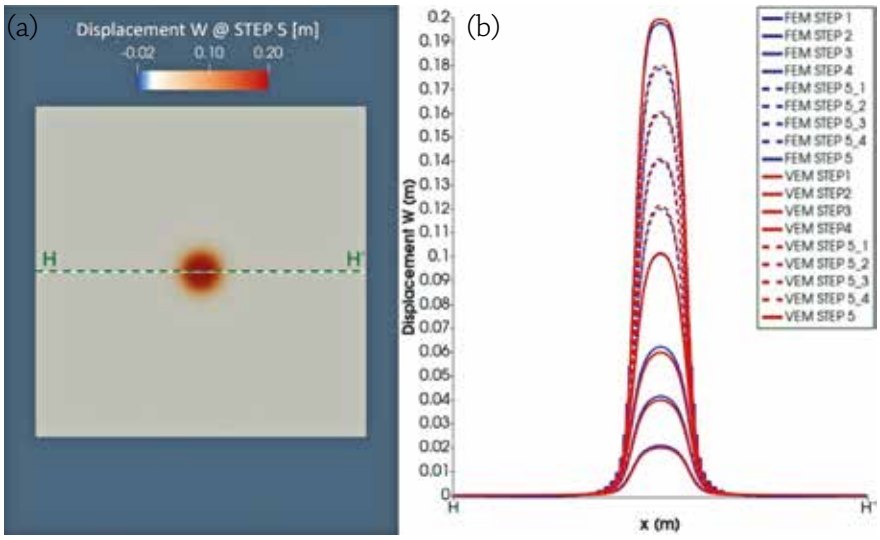


Fig. 10 – (a) Top view of the model. The colormap refers to the displacement component W along the z-axis expressed in m at the last loading step. (b) comparison of the subsidence along the dotted green segment HH' in (a).

along the x-direction in figures 11a and 11b, respectively. Due to the radial symmetry of the problem the y-component is not shown. A comparison is performed also on the effective stress map. As an example, the $\sigma'_{xx}$ map calculated at the final equilibrium (i.e. when the whole $\Delta p$ is imposed) and the evolution along the HH' section are shown in figures 12a and 12b, respectively.

Agreement among the solutions is also verified through a section along the vertical segment OO'. The comparison of the vertical component of displacement (W) is depicted in figure 13, while $\Delta\sigma'_{zz}$, i.e. the variation of the zz-component of the effective stress tensor, between step 4 and step 5 is shown in figure 14.

## 4. Conclusion

In this paper, we explore the possibility to describe the geomechanical behavior of underground formations used for fluid storage through the application of VEM to conforming mesh for the resolution of stress-strain equilibrium equations. Under the hypothesis of small deformations, the solution algorithm for an ILE constitutive law coupled with Mohr-Coulomb perfectly plastic yield criterion is implemented and tested on a scenario with realistic parameters and simplified geometry. In particular it is worthwhile to mention the implementation of a regularization of the yield function which is C2 continuous in all stress states as proposed by (Abbo *et al.*, 2011) and the integration of a backtracking algorithm in the two nested Newton's iteration in order to enforce convergence. Results are compared with the solution of a first-order FEM obtained from a commercial solver, showing a good agreement in terms of displacement and stress maps. The added value of the current implementation is given by the promising stabilization term associated with VEM projectors in the case of the non-linear constitutive model. The obtained results allow us to expand the analysis to more complex geometries through the introduction of polyhedral cells (for which VEM generalization is straightforward) and the simulation of topological discontinuities such as faults.

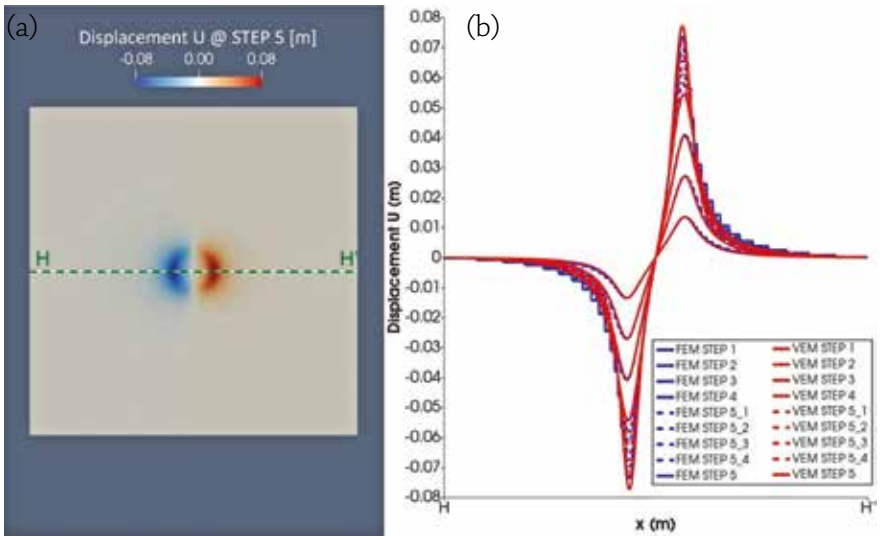


Fig. 11 – (a) Top view of the model. The colormap refers to the displacement component U along the x-axis expressed in m at the last loading step. (b) comparison of the evolution of the x-axis displacement component U along the dotted green segment HH' in (a).

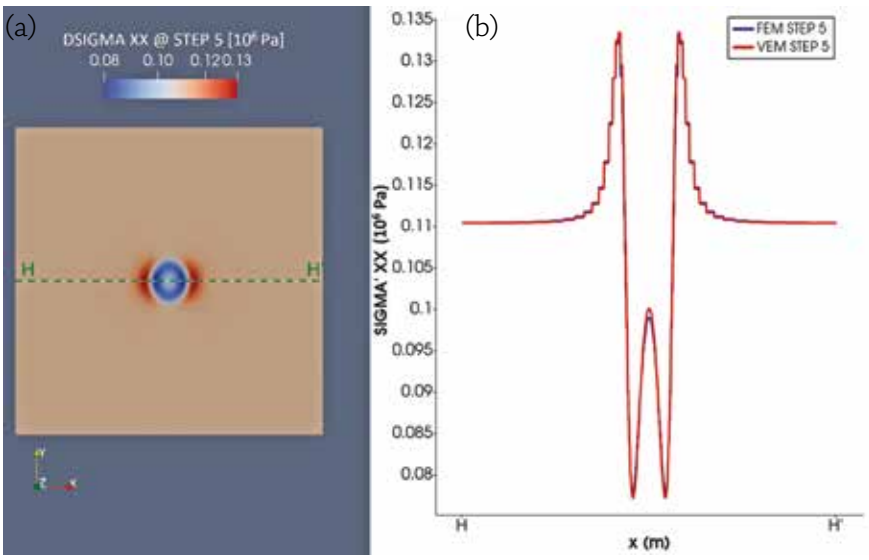


Fig. 12 – (a) Top view of the model. The colormap refers to the xx effective stress component expressed in MPa after the last loading step. (b) comparison of the xx effective stress component along the dotted green segment HH' in (a).

## References

Abbo, A.J., Lyamin, A.V., Sloan, S.W., Hambleton, J.P., (2011). A C2 continuous approximation to the Mohr-Coulomb yield surface. International Journal of Solids and Structures 48, pp. 3001-3010.

Abbo, A.J., Sloan, S.W., (1995). A smooth hyperbolic approximation to the Mohr-Coulomb yield criterion. Computers & Structures 54, pp. 427-441. https://doi.org/10.1016/0045-7949(94)00339-5

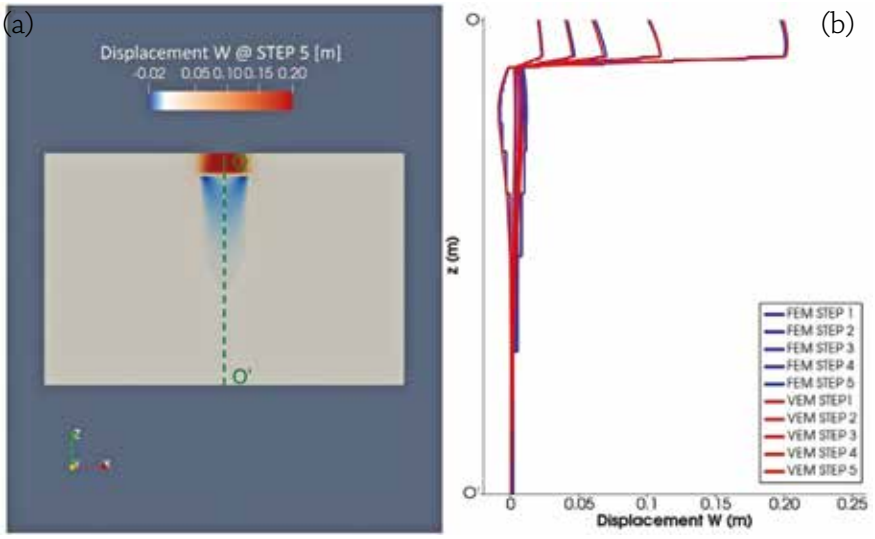


Fig. 13 – (a) Section orthogonal to the y-axis of the model. The colormap refers to the displacement component W along the z-axis expressed in m at the last loading step. A scale factor of 2 is applied to the z-axis. (b) comparison of the evolution of the z-axis displacement component W along the dotted green segment OO' in (a).

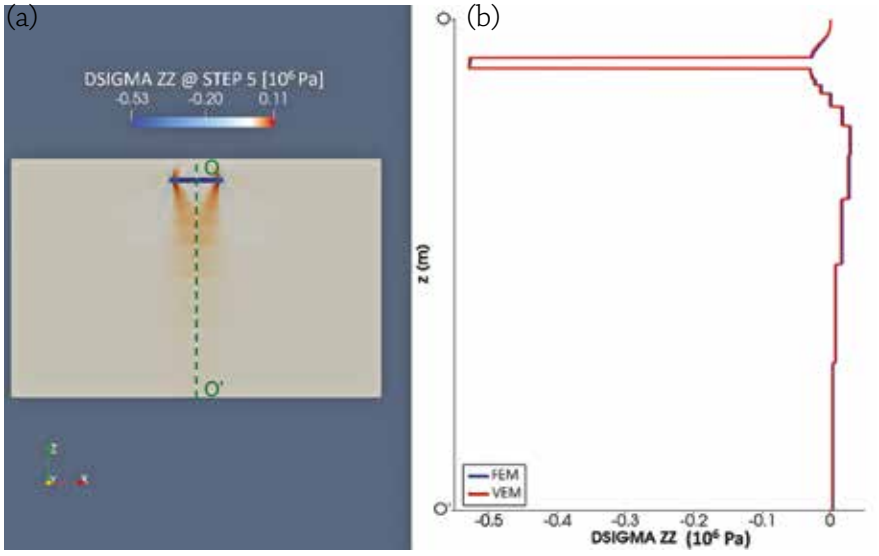


Fig. 14 – (a) Section orthogonal to the y-axis of the model. The colormap refers to the zz-effective stress variation ($\Delta\sigma'_{zz}$) between loading step 5 and loading step 4. A scale factor of 2 is applied to the z-axis. (b) comparison of the zz-effective stress variation ($\Delta\sigma'_{zz}$) between loading step 5 and loading step 4 along the dotted green segment OO' in (a).

Ahmad, B., Alsaedi, A., Brezzi, F., Marini, L.D., Russo, A., (2013). Equivalent projectors for virtual element methods. Computers & Mathematics with Applications 66, pp. 376-391. https://doi.org/10.1016/j.camwa.2013.05.015

Beirão da Veiga, L., Brezzi, F., Cangiani, A., G, M., Marini, L.D., Russo, A., 2013a. Basic principles of virtual element methods. Mathematical Models and Methods in Applied Sciences 23, pp. 199-214. https://doi.org/10.1142/S0218202512500492

Beirão da Veiga, L., Brezzi, F., Marini, L.D., Russo, A., (2016). Virtual Element Method for general second-order elliptic problems on polygonal meshes. Mathematical Models and Methods in Applied Sciences 26, pp. 729-750. https://doi.org/10.1142/S0218202516500160

Beirão da Veiga, L., Brezzi, F., Marini, L.D., Russo, A., (2014). The Hitchhiker's Guide to the Virtual Element Method. Mathematical Models and Methods in Applied Sciences 24, pp. 1541-1573. https://doi.org/10.1142/S021820251440003X

Beirão da Veiga, L., F, B., D, M.L., (2013b). Virtual Elements for Linear Elasticity Problems. SIAM Journal on Numerical Analysis 51, pp. 794-812. https://doi.org/10.1137/120874746

Beirão da Veiga, L., Lovadina, C., Mora, D., (2015). A Virtual Element Method for elastic and inelastic problems on polytope meshes. Computer Methods in Applied Mechanics and Engineering 295, pp. 327-346. https://doi.org/10.1016/j.cma.2015.07.013

Beirão da Veiga, L., Lovadina, C., Russo, A., (2017). Stability analysis for the virtual element method. Math. Models Methods Appl. Sci. 27, pp. 2557-2594. https://doi.org/10.1142/S021820251750052X

Bellini, R., Bassani, I., Vizzarro, A., Azim, A.A., Vasile, N.S., Pirri, C.F., Verga, F., Menin, B., (2022). Biological Aspects, Advancements and Techno-Economical Evaluation of Biological Methanation for the Recycling and Valorization of CO2. Energies 15. https://doi.org/10.3390/en15114064

Benedetto, M.F., Berrone, S., Pieraccini, S., Scialà, S., (2014). The virtual element method for discrete fracture network simulations. Computer Methods in Applied Mechanics and Engineering 280, pp. 135-156. http://dx.doi.org/10.1016/j.cma.2014.07.016

Benetatos, C., Bocchini, S., Carpignano, A., Chiodoni, A., Cocuzza, M., Deangeli, C., Eid, C., Ferrero, D., Gerboni, R., Giglio, G., Lamberti, A., Marasso, S., Massimiani, A., Menin, B., Moscatello, A., Panini, F., Peter, C., Pirri, F., Quaglio, M., Rocca, V., Rovere, A., Salina Borello, E., Serazio, C., Uggenti, A.C., Vasile, N., Verga, F., Viberti, D., (2021). How underground systems can contribute to meet the challenges of energy transition. GEAM. Geoingegneria Ambientale e Mineraria 58, pp. 65-80. https://doi.org/10.19199/2021.163-164.1121-9041.065

Benetatos, C., Catania, F., Giglio, G., Pirri, C.F., Raeli, A., Scaltrito, L., Serazio,

C., Verga, F., (2023). Workflow for the Validation of Geomechanical Simulations through Seabed Monitoring for Offshore Underground Activities. JMSE 11, 1387. https://doi.org/10.3390/jmse11071387

Benetatos, C., Codegone, G., Deangeli, C., Giani, G.P., Gotta, A., Marzano, F., Rocca, V., Verga, F., (2017). Guidelines for the study of subsidence triggered by hydrocarbon production. GEAM 152, pp. 85-96.

Benetatos, C., Codegone, G., Ferraro, C., Mantegazzi, A., Rocca, V., Tango, G., Trillo, F., (2020). Multidisciplinary Analysis of Ground Movements: An Underground Gas Storage Case Study. Remote Sensing 12. https://doi.org/10.3390/rs12213487

Benlalam, N., Serazio, C., Rocca, V., (2022). VEM application to geomechanical simulations of an Italian Adriatic offshore gas storage scenario. GEAM 165, pp. 41-49. https://doi.org/10.19199/2022.165.1121-9041.041

Berrone, S., Borio, A., D'Auria, A., (2021a). Refinement strategies for polygonal meshes applied to adaptive VEM discretization. Finite Elements in Analysis and Design 186, 103502. https://doi.org/10.1016/j.finel.2020.103502

Berrone, S., Borio, A., D'Auria, A., Scialò, S., Vicini, F., (2021b). A robust VEM-based approach for flow simulations in poro-fractured media. Math. Models Methods Appl. Sci. 31, pp. 2855-2885. https://doi.org/10.1142/S0218202521500639

Berrone, S., Raeli, A., (2022). Efficient partitioning of conforming virtual element discretizations for large scale discrete fracture network flow parallel solvers. Engineering Geology 306, 106747. https://doi.org/10.1016/j.enggeo.2022.106747

Biot, M.A., (1941). General Theory of Three-Dimensional Consolidation. Journal of Applied Physics 12, pp. 155-164. https://doi.org/10.1063/1.1712886

Bouteca, M., Guéguen, Y., (1999). Mechanical Properties of Rocks: Pore Pressure and Scale Effects. Oil & Gas Science and Technology – Rev. IFP 54, pp. 703-714. https://doi.org/10.2516/ogst:1999060

Caporali, A., Braitenberg, C., Montone, P., Rossi, G., Valensise, G., Viganò, A., Zurutuza, J., (2018). A quantitative approach to the loading rate of seismogenic sources in Italy. Geophysical Journal International 213, pp. 2096-2111. https://doi.org/10.1093/gji/ggy112

Codegone, G., Rocca, V., Verga, F., Coti, C., (2016). Subsidence Modeling Validation Through Back Analysis for an Italian Gas Storage Field. Geotechnical and Geological Engineering 34, pp. 1749-1763. https://doi.org/10.1007/s10706-016-9986-9

Coti, C., Rocca, V., Sacchi, Q., (2018). Pseudo-Elastic Response of Gas Bearing Clastic Formations: An Italian Case Study. Energies 11. https://doi.org/10.3390/en11092488

Coulomb, C.A., (1776). Essai sur une application des règles de maximis & minimis à quelques problèmes de statique, relatifs à l'architecture. Paris: De l'Imprimerie Royale.

Ferronato, M., Castelletto, N., Gambolati, G., Janna, C., Teatini, P., (2013). Il cycle compressibility from satellite measurements. Géotechnique 63, pp. 479-486. https://doi.org/10.1680/geot.11.P.149

Fibbi, G., Del Soldato, M., Fanti, R., (2023). Review of the Monitoring Applications Involved in the Underground Storage of Natural Gas and CO2. Energies 16. https://doi.org/10.3390/en16010012

Fjær, E., Holt, R.M., Horsrud, P., Risnes, R., Raaen, A.M., (2008). Petroleum Related Rock Mechanics, Developments in Petroleum Science. Elsevier Science & Technology.

Gain, A.L., Talischi, C., Paulino, G.H., (2014). On the Virtual Element Method for three-dimensional linear elasticity problems on arbitrary polyhedral meshes. Computer Methods in Applied Mechanics and Engineering 282, pp. 132-160. https://doi.org/10.1016/j.cma.2014.05.005

Geertsma, J., (1973). Land Subsidence Above Compacting Oil and Gas Reservoirs. Journal of Petroleum Technology 25, pp. 734-744. https://doi.org/10.2118/3730-PA

Guennebaud, G., Jacob, B., *et al.*, (2010). Eigen v3.

Han, D.J., Chen, W.F., (1987). Constitutive Modeling in Analysis of Concrete Structures. J. Eng. Mech. 113, pp. 577-593. https://doi.org/10.1061/(ASCE)0733-9399(1987)113:4(577)

Hematpur, H., Abdollahi, R., Rostami, S., Haghighi, M., Blunt, M.J., (2023). Review of underground hydrogen storage: Concepts and challenges. Advances in Geo-Energy Research 7, pp. 111-131. https://doi.org/10.46690/ager.2023.02.05

IEA, (2020). CCUS in Clean Energy Transitions, Energy Technology Perspectives. Paris, https://www.iea.org/reports/ccus-in-clean-energy-transitions, License: CC BY 4.0.

Krabbenhøft, K., (2002). Basic computational plasticity. University of Denmark.

Lancellotta, R., (2008). Geotechnical Engineering, 2nd ed. CRC Press.

Liu, E., Lu, X., Wang, D., (2023). A Systematic Review of Carbon Capture, Utilization and Storage: Status, Progress and Challenges. Energies 16, pp. 1-48.

Miocic, J., Heinemann, N., Edlmann, K., Scafidi, J., Molaei, F., Alcalde, J., (2023). Underground hydrogen storage: a review. SP 528, pp. 73-86. https://doi.org/10.1144/SP528-2022-88

Nayak, G.C., Zienkiewicz, O.C., (1972). Convenient Form of Stress Invariants for Plasticity. J. Struct. Div. 98, pp. 949-954. https://doi.org/10.1061/JSDEAG.0003219

Neto, E.A. de S., Peric, D., Owen, D.R.J., (2008). Computational Methods for Plasticity: Theory and Applications. Wiley.

Paluszny, A., Graham, C.C., Daniels, K.A., Tsaparli, V., Xenias, D., Salimzadeh, S., Whitmarsh, L., Harrington, J.F., Zimmerman, R.W., (2020). Caprock integrity and public perception studies of carbon storage in depleted hydrocarbon reservoirs. International Journal of Greenhouse

Gas Control 98, 103057. https://doi.org/10.1016/j.ijggc.2020.103057
Ramesh Kumar, K., Honorio, H., Chandra, D., Lesueur, M., Hajibeygi, H., (2023). Comprehensive review of geomechanics of underground hydrogen storage in depleted reservoirs and salt caverns. Journal of Energy Storage 73, 108912. https://doi.org/10.1016/j.est.2023.108912
Serazio, C., (2021). Application of Virtual Element Methods for geomechanical assessment of fluid storage in deep geological formations. Politecnico di Torino, Torino.
Shewchuk, J.R., (1996). Triangle: Engineering a 2D Quality Mesh Generator and Delaunay Triangulator, in: Lin, M.C., Manocha, D. (Eds.), Applied Computational Geometry Towards Geometric Engineering: FCRC'96 Workshop, WACG'96 Philadelphia, PA, May 27-28, 1996 Selected Papers. Springer Berlin Heidelberg, Berlin, Heidelberg, pp. 203-222. https://doi.org/10.1007/BFb0014497
Shi, Z., Jessen, K., Tsotsis, T.T., (2020). Impacts of the subsurface storage of natural gas and hydrogen mixtures. International Journal of Hydrogen Energy 45, 8757-8773. https://doi.org/10.1016/j.ijhydene.2020.01.044
Szymanski, A., (1996). Chapter 5 Analysis of subsoil deformations, in: Developments in Geotechnical Engineering. Elsevier, pp. 181-238. https://doi.org/10.1016/S0165-1250(96)80008-3
Teatini, P., Castelletto, N., Ferronato, M., Gambolati, G., Janna, C., Cairo, E., Marzorati, D., Colombo, D., Ferretti, A., Bagliani, A., Bottazzi, F., (2011). Geomechanical response to seasonal gas storage in depleted reservoirs: A case study in the Po River basin, Italy. Journal of Geophysical Research: Earth Surface 116. https://doi.org/10.1029/2010JF001793
Terzaghi, K., (1936). The Shearing Resistance of Saturated Soils and the Angle between the Planes of Shear. Presented at the 1st International Conference on Soil Mechanics and Foundation Engineering, pp. 54-56.
van Huyssteen, D., Rivarola, F.L., Etse, G., Steinmann, P., (2022). On mesh refinement procedures for the virtual element method for two-dimensional elastic problems. Computer Methods in Applied Mechanics and Engineering 393, 114849. https://doi.org/10.1016/j.cma.2022.114849
Vasile, N.S., Bellini, R., Bassani, I., Vizzarro, A., Abdel Azim, A., Coti, C., Barbieri, D., Scapolo, M., Viberti, D., Verga, F., Pirri, F., Menin, B., (2023). "Innovative high pressure/high temperature, multi-sensing bioreactors system for microbial risk assessment in underground hydrogen storage." International Journal of Hydrogen Energy S0360319923053934. https://doi.org/10.1016/j.ijhydene.2023.10.245
Velez, G.C., Mesa, F., Cardenas Alzate, P.P., (2018). Linear search optimization through the Armijo rule method. ces 11, pp. 771-778. https://doi.org/10.12988/ces.2018.8121
Verga, F., (2018). What's Conventional and What's Special in a Reservoir Study for Underground Gas Storage. Energies 11. https://doi.org/10.3390/en11051245
Zang, A., Stephansson, O., Heidbach, O., Janouschkowetz, S., (2012). World Stress Map Database as a Resource for Rock Mechanics and Rock Engineering. Geotechnical and Geological Engineering 30, pp. 625-646. https://doi.org/10.1007/s10706-012-9505-6

## *Declaration of Interest*

The authors declare no conflict of interest.

## *Acknowledgements*

The authors are thankful to the Ministry of Ecological Transition, Energy Department, General Directorate for Infrastructure and Security (previously Ministry of the Economic Development, General Directorate for Infrastructures and Security of Energy and Geomining Systems, and currently Ministry of Environment and Energy Security) for their support of this research.